Fibrin Clot Extension on Zirconia Surface for Dental Implants: A Quantitative In Vitro Study

Tonino Traini, DDS, PhD;*,† Sergio Caputi, MD, DDS;* Enrico Gherlone, MD, DDS;†
Marco Degidi, MD, DDS;‡ Adriano Piattelli, MD, DDS*

ABSTRACT

Purpose: The surface chemical and physical properties of materials used for implants have a major influence on blood clot organization. This study aims to evaluate the blood clot extension (*bce*) on zirconia and titanium. *bce* was measured in association to surface roughness (*Ra*) and static contact angle (θ).

Materials and Methods: Forty disk-shaped samples of sandblasted yttria tetragonal zirconia polycrystal (*sb-YTZP*), machined titanium (*m-Ti*), and sandblasted, high-temperature, acid-etched titanium (*p-Ti*) were used in the present study. About 0.2 mL of human blood, immediately dropped onto the specimen's surface and left in contact for 5 minutes at room temperature, was used to measure the *bce*. Specimens were observed under confocal scanning laser and scanning electron microscopes.

Results: The *bce* (mean $\times 10^7 \pm$ standard deviation [SD] $\times 10^6$ μm^2) was 2.97 ± 6.68 for *m-Ti*, 5.64 ± 6.83 for *p-Ti*, and 3.61 ± 7.67 for *sb-YTZP*. *p-Ti* samples showed a significantly higher *bce*. *Ra* (mean ± SD [μm]) was 0.56 ± 0.7 for *m-Ti*, 3.78 ± 0.8 for *p-Ti*, and 2.68 ± 0.6 for *sb-YTZP*. The difference was not significant between *sb-YTZP* and *p-Ti*. θ (mean ± SD) was 55.6 ± 5.6 for *m-Ti*, 48.7 ± 2.8 for *sb-YTZP*, and 38.0 ± 2.2 for *p-Ti*. The difference was not significant between *m-Ti* and *sb-YTZP*.

Conclusions: The *sb-YTZP* demonstrated a significantly lesser amount of *bce* compared with *p-Ti* specimens, notwithstanding that any significant difference was present between *Ra* and θ.

KEY WORDS: blood–material interaction, dental/endosteal implant, fibrin, surface characterization

INTRODUCTION

Dental implants are exposed, after insertion, to the patient's blood; the interactions of the foreign implant material with the implant surface will influence the extent of the fibrin network formation and of the acute inflammatory processes.[1,2] Implant surface topography in the nanoscale to microscale will positively affect the reactions of the peri-implant bone[3] and the bone growth processes.[4] Chemistry and topography of dental implant surfaces were able to influence interactions with all blood components.[5,6] Osseointegration might, then, be directly influenced by the physicochemical properties of the implant surface.[5,7] Titanium is the material of choice for dental implants and has also been reported to be highly thrombogenic.[8] Because of the material's tooth-like color and its biocompatibility, yttria tetragonal zirconia polycrystal (YTZP) has become an attractive alternative to titanium for implants.[9–12] YTZP is a bio-inert material and shows minimal ion release compared with metallic implants. Recently, Özkurt and Kazazoğlu[13] in a literature review reported YTZP as an alternative materials for dental implants; Oliva and colleagues[14] considered zirconia a viable alternative material for dental implants on the basis of a human clinical trial on eight hundred thirty-one zirconia dental implants with different roughness surfaces. Several authors have studied the factors related to surface properties, such as surface roughness, chemistry, and surface

*Department of Medical, Oral and Biotechnological Sciences, University of Chieti-Pescara, Chieti-Pescara, Italy; †Department of Dentistry, San Raffaele Hospital, Vita Salute University, Milano, Italy; ‡private practice, Bologna, Italy

Reprint requests: Dr. Tonino Traini, Department of Dentistry, Vita Salute University, San Raffaele Hospital, via Olgettina 58, 20132 Milano, Italy; e-mail t.traini@gmail.com

DOI 10.1111/cid.12038

morphology.[15–19] The ideal surface topography is, however, still unknown.[15] The sensitivity of the cytoskeleton to organize in relationship to the surface microstructure seems to be high with an intermediate level of roughness and low in relatively smooth and extremely rough surfaces.[17] In 2003, Kim and colleagues[20] evaluated the response of the peri-implant bone in blasted and blasted/etched implants: a higher quantity of bone in contact with blasted/etched implants in the primary healing period, while, after 3 months, no significant differences were found between the two groups. The same authors also suggested that with blasting and blasting/etching procedures, it would be possible to obtain implant surfaces with different roughnesses and oxide thicknesses.[20] Di Iorio and colleagues[21] reported a significant fibrin clot retention for titanium implants with a microstructured surface. Sul and colleagues[22] highlighted the importance of the oxide thickness for the bone reactions; they found that an oxide thickness of 600 to 1000 nm allowed a better bone-to-implant surface reaction. Buser and colleagues[23] and Larsson and colleagues[24] stated that bone-to-metal contact improved as implant surface becomes rougher. Nygren and colleagues[25] and Keselowsky and colleagues[16] reported that, within a short time of contact, host plasma proteins were adsorbed on the implant surface. This biofilm, formed by immunoglobulins, vitronectin, fibrinogen, and fibronectin, seems to function as cell-adhesion-promoting and cell-activating ligands.[16] Other studies[26,27] underlined the relationship between the surface properties of the titanium and the adsorbed protein layer. Sevastianov[28] reported that albumin was adsorbed on the surface, while Tang and Eaton[29] showed that adsorbed fibrinogen played a relevant role in the activation of the inflammatory response of the bone tissue. When the plasma proteins contact the metal surface, there is an activation of the protein cascade, i.e., coagulation, fibrinolysis, and complement system.[30–34] The coagulation is the first step of bone healing. Fibrinogen is the soluble blood precursor of the fibrin clot.[35] Both fibrinogen and fibrin are important in the clot formation, cellular and matrix interactions, fibrinolysis, inflammation, and wound healing.[35] Fibrin, formed at the site of injury, provides the temporary matrix, supporting the initial endothelial cell response for vessel repair.[36] Formation of a thrombus on biomaterials has been reported to be correlated with charge transfer from the inactive state of fibrinogen to the surface of the biomaterial[37]; fibrinogen tends to decompose to fibrinomonomer and fibrinopeptides. The monomers will produce fibrin, before cross-linking to an irreversible thrombus. Moreover, it has been proven that fibrinogen had an electronic structure similar to an intrinsic semiconductor with a band gap of 1.8 eV,[37] and when fibrinogen was adsorbed onto the titanium oxide film, a junction was formed by the transfer of electrons, improving the blood biocompatibility. Over zirconia, this process was less effective because the band gap was >5 eV. Titanium has three types of oxide crystal structure: (1) anatase, (2) rutile, and (3) brookite. The band gap value for the anatase type is 3.20 eV, for the rutile type is 3.02 eV, and for the brookite type is 2.96 eV.[38] Fibrin is a material rapidly invaded, remodeled, and replaced by a cell-associated proteolytic activity.[39] The fibrin structure is quite loose at the beginning of the process, but after 5 minutes, a tighter structure will be formed under the influence of factor XIII (fibrin-stabilizing factor), converting the fibrin monomer into a polymer.[40] The formation of a fibrin scaffold is crucial because it represents the pathway that helps the osteogenic cells to reach the implant surface[41]; the osteogenic cells will not interact with the titanium implant surface, but with a blood-modified titanium oxide surface.[42] According to the knowledge of the present authors, no information was present in the dental literature on the relationship between zirconia and fibrin clot.

The aim of the present study was a quantitative evaluation of the in vitro fibrin clot extension on zirconia and different titanium surfaces.

MATERIALS AND METHODS

General Procedure

A total of 43 disk-shaped specimens presenting a diameter of 5 mm and a thickness of 2 mm were used in the present study. Three different surface topographies and two types of implant materials were investigated. The specimens were divided as follows: 11 titanium specimens with machined surface (*m-Ti*) (DENTSPLY Implants Manufacturing GmbH, Mannheim, Germany); 11 titanium specimens with plus® surface (*p-Ti*) (DENTSPLY Implants Manufacturing GmbH); and 21 YTZP specimens with grit-blasted surface (*sb-YTZP*) (Diazir, Diadem SAS, Louey, France). The *m-Ti* specimens were obtained with a turning procedure (Figure 1); *p-Ti* disks were grit blasted with large grit

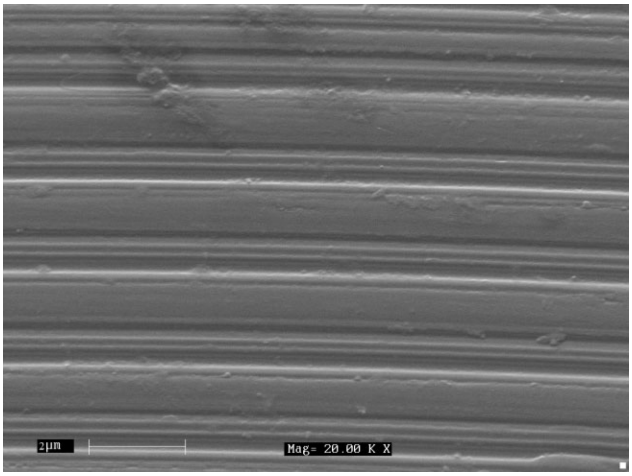

Figure 1 Scanning electron microscope image (×20.000) of machined titanium surface (*m-Ti*).

aluminum oxide particles (350–500 µm) and acid etched in high-temperature computer-controlled processes. The specific process used to produce the plus surface was considered a company proprietary process (Figure 2); the *sb-YTZP* specimens were obtained with a grit-blasting procedure with aluminum oxide particles (250–500 µm) at 5 bars followed by cleaning procedure in an ultrasonic bath containing 96% ethanol for 10 minutes (Figure 3).

Surface Characterization

A Zeiss confocal laser scanning microscope (CLSM) 510 META (Zeiss, Jena, Germany) using a 15-mW argon laser with a 40× / 1.2 finite numerical aperture (NA) objective and a 166-µm pinhole, was used to numerically describe the appearance of the surface topography.

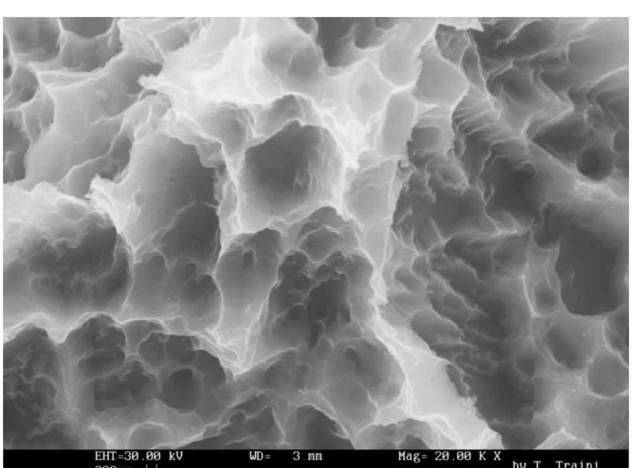

Figure 2 Scanning electron microscope image (×20.000) of plus titanium surface (*p-Ti*).

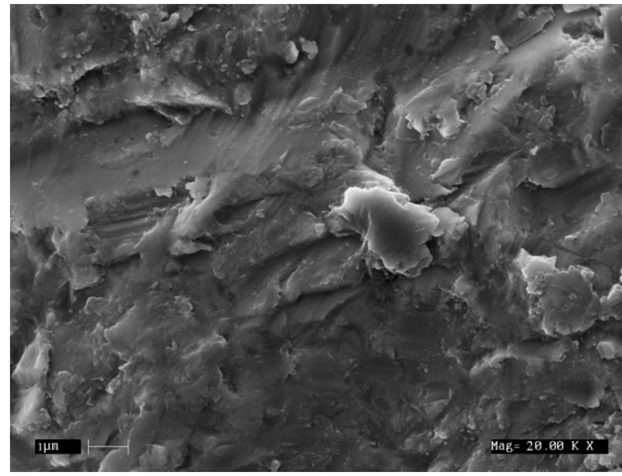

Figure 3 Scanning electron microscope image (×20.000) of sandblasted zirconia surface (*sb-YTZP*).

Three specimens for each of the three different surfaces were evaluated, while the area of measurement was 20 × 20 µm. The surface parameter evaluated was the average height deviation value (*Ra*).

Contact Angle Measurements

Contact angles (θ), i.e., the angle between the tangent to a water drop and the solid surface at the three-phase liquid : solid : air meeting point,[43] were analyzed for each ($n = 3$) of the three different surfaces considered in the present study. The static contact angle was used as a measure of surface hydrophobicity. Sessile water drops with a volume of 10 µL were placed at the flat material surfaces under the same environmental conditions. The contact angle with water was measured from photographs, using Image-Pro Plus version 6.0 (Media Cybernetics Inc., Bethesda, MD, USA).

Blood Samples

Venous blood was drawn, with permission, from three adult healthy volunteers not on medication and with a bleeding time comprised between 2 and 3 minutes (Duke's assay). For all specimens, the human whole blood, without any addition of anticoagulant, was immediately dropped (0.1 mL) onto the surface of each specimen using a syringe. As blood drawn was instantly used for the experiment, the first drops were not discarded. About 0.1 mL of blood was sufficient to cover the entire specimen surface. Contact time was 5 minutes at room temperature; thereafter, the samples were rinsed with saline solution and fixed in a buffered solution at pH 7.2 of 2.5% of glutaraldehyde and 2.5% of paraformaldehyde. Samples were washed again with buffer and dehydrated in an ascending alcohol series.

Measurements of Blood Clot

Samples belonging to the three different groups ($n = 25$) were investigated under both CLSM and scanning electron microscope (SEM).

For SEM surface characterization and measure, the specimens underwent critical point drying in Emitech K 850 (Emitech Ltd., Ashford, Kent, UK) than were mounted onto aluminum stubs, sputter gold coated in Emitech K 550 (Emitech Ltd.), and imaged in a Cambridge Stereoscan 200 (Cambridge Instrument Company Ltd, Cambridge, England) equipped with tetra-solid-state detector for back-scattered electrons (BSEs). The BSE signal was used because it is generated from about a 0.5-μm-thick surface layer of the specimen and because the number of emitted electrons was strongly dependent on the atomic number of the specimen. SEM operating conditions included 15- to 30-kV accelerating voltage, 14- to 32-mm working distance, and 0.75-nA probe current. The BSE images were captured with nine scans using a line average technique.

From each sample, 10 random micrographs at a magnification of ×1000 were collected in .tif format with $N \times M$ (1024 × 768) grid of pixels. To measure the areas covered by the fibrin clot, the images were analyzed using Image-Pro Plus 6.0. To ensure accuracy, the software was calibrated for each experimental image using a software feature named "Calibration Wizard," which reports the number of pixel between two selected points (diameter of the disks). The linear remapping of the pixel numbers was used to calibrate the distance in microns. The measurements were drawn in square micrometer; individual average values were calculated per sample, then, group average values were calculated, summarizing the individual values.

Statistics

One person performed all of the measurements. Carrying out two measurements for each index controlled intra-examiner variability. When the difference in the two performed readings exceeded 5% for the same index, the measure was repeated. Statistical analysis was performed by means of a computerized statistical package (Sigma Stat 3.5, SPSS Inc., Ekrath, Germany). The data were analyzed with descriptive statistics to assess whether they had a normal distribution. One-way analysis of variance (ANOVA) and Holm-Sidak tests were used to evaluate the overall significance and to perform all pairwise comparisons of the mean responses, respectively. A p-value of <.05 was considered statistically significant.

RESULTS

Under SEM, the *m-Ti* samples (Figure 1) showed the presence of typical machining grooves produced by the manufacturing instruments. The *p-Ti* samples (Figure 2) showed the presence of a macroscopic level of roughness in the dimensions of 100 μm. There was also a second level of grooves of about 20 to 70 μm; these grooves were set around smaller grooves with different shapes. These second- and third-level grooves appeared to have very sharp edges. The *sb-YTZP* samples (Figure 3) showed a rough surface produced by the blasting procedure. The surface was irregular with many depressions, peaks, and small diameter indentations.

The surface roughness (*Ra*), measured under CLSM (Figure 4, A–C), was 0.56 ± 0.7 μm for *m-Ti*, 2.68 ± 0.6 μm for *sb-YTZP*, and 3.78 ± 0.8 μm for *p-Ti*. The differences appeared to be statistically significant

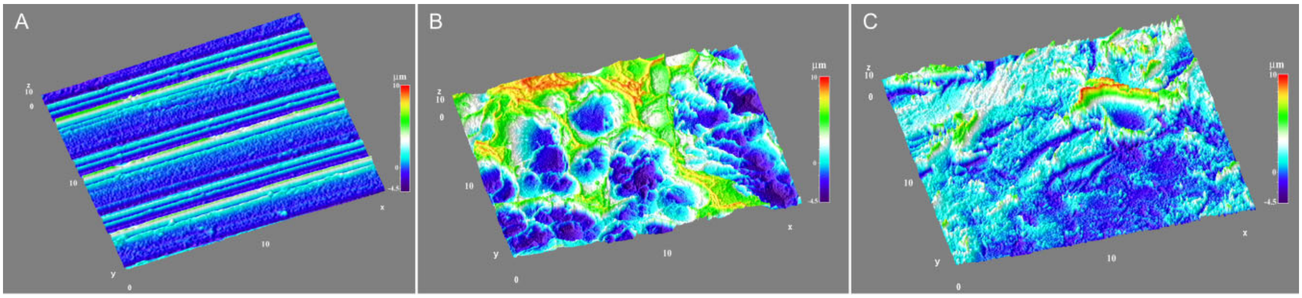

Figure 4 Three-dimensional reconstructions of surface topographies from *Ra* values under confocal laser scanning microscope. (A) *m-Ti* specimen; (B) *p-Ti* specimen; and (C) *sb-YTZP* specimen.

TABLE 1 Surface Roughness of Tested Materials (Mean ± SD)

Groups	*n*	*Ra* (µm)	SD (µm)
m-Ti	3	0.56*	0.7
p-Ti	3	3.78*†	0.8
sb-YTZP	3	2.68*†	0.6

*Statistically significant.
†Not statistically significant at $\alpha < 0.05$ and $1 - \beta = 0.970$.
One-way ANOVA and Holm-Sidak methods.
ANOVA = analysis of variance; m-Ti = titanium specimens with machined surface; p-Ti = titanium specimens with plus surface; sb-YTZP = yttria tetragonal zirconia polycrystal specimens with sand-blasted surface; SD = standard deviation.

TABLE 2 Contact Angles (θ) of Tested Materials (Mean ± SD)

Groups	*n*	Mean (°)	SD (°)
m-Ti	3	55.66*†	5.6
p-Ti	3	38.00*	2.2
sb-YTZP	3	48.70*†	2.8

*Statistically significant.
†Not statistically significant at $\alpha < 0.05$ and $1 - \beta = 0.965$.
One-way ANOVA and Holm-Sidak methods.
ANOVA = analysis of variance; m-Ti = titanium specimens with machined surface; p-Ti = titanium specimens with plus surface; sb-YTZP = yttria tetragonal zirconia polycrystal specimens with sand-blasted surface; SD = standard deviation.

between both *p-Ti* and *sb-YTZP versus m-Ti* ($p < .05$), while no statistically significant difference was seen between *p-Ti* and *sb-YTZP* ($p > .05$) (Table 1).

The contact angles (θ), measured in static conditions (Figure 5, A–C), was 55.66 ± 5.6 for *m-Ti*, 38.00 ± 2.2 for *p-Ti*, and 48.70 ± 2.8 for *sb-YTZP*. Between *m-Ti* and *sb-YTZP*, no statistically significant difference was seen ($p > .05$), while for the *p-Ti* group, a significant decrease of θ ($p < .05$) was present (Table 2).

Quantitative analysis of blood clot extension (*bce*) (Figure 6) showed the following results: in *m-Ti* samples, *bce* was $2.97 \times 10^7 \pm 6.68 \times 10^6\ \mu m^2$; in *p-Ti* samples, *bce* was $5.64 \times 10^7 \pm 6.83 \times 10^6\ \mu m^2$; while in *sb-YTZP* samples, *bce* was $3.61 \times 10^7 \pm 7.67 \times 10^6\ \mu m^2$. ANOVA discovered a significant difference among the groups ($p < .001$). The Holm-Sidak multiple comparison procedure revealed that the *bce* of *p-Ti* samples was statistically higher compared with both *m-Ti* and *sb-YTZP* samples ($p < .05$). No significant difference was noted between *m-Ti* and *sb-YTZP* samples ($p > .05$) (Table 3). SEM image comparison among all groups of samples showed also qualitative differences in *bce* organization. SEM images of *m-Ti* sample (Figure 7) showed a thin fibrin scaffold attached to the specimen surface with some red blood cells attached but not trapped by the fibrin filaments. Moreover, part of the specimen surface was visible and the fibrin scaffold appeared to be two dimensional. The *sb-YTZP* specimen (Figure 8), on the other hand, despite a tridimensional organization of the fibrin scaffold, showed only very few red blood cells trapped in the fibrin scaffold. Finally, the *p-Ti* specimen (Figure 9) demonstrated a very intricate tridimensional organization of the fibrin scaffold with some red blood cells attached and trapped by the implant surface microconcavities.

DISCUSSION

Hemocompatibility is a key factor in the successful design and function of a medical device. When a foreign material comes into contact with blood, changes occur in both the hemostatic and inflammatory systems.[25,44] Thus, it should not be surprising that the adhesion of cells to biomaterial surfaces is a crucial step in the tissue/biomaterial integration.[16] This adhesive interaction anchors cells that activate several intracellular signaling pathways to direct cell viability, proliferation, and differentiation.[16] The tissue response to rougher surfaces seems to be better than that observed around smoother

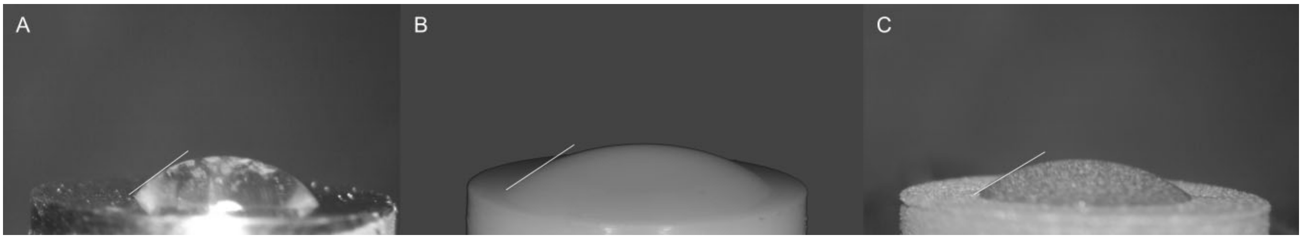

Figure 5 Measure of the surface hydrophobicity (contact angles) by sessile water drops. (A) *m-Ti* specimen; (B) *sb-YTZP* specimen; and (C) *p-Ti* specimen.

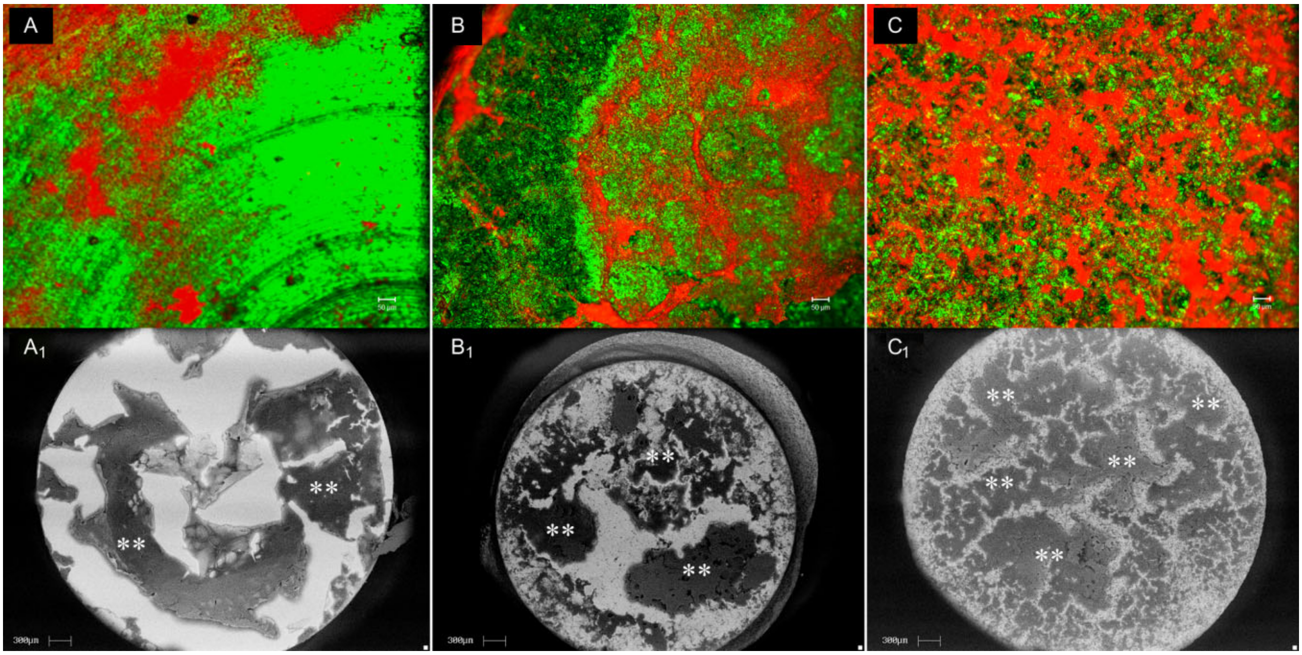

Figure 6 Evaluation of blood clot extension (*bce*). Under confocal laser scanning microscope (×200), *bce* appeared in red and the specimen surface in green. (A) *m-Ti* specimen; (B) *sb-YTZP* specimen; and (C) *p-Ti* specimen. Under scanning electron microscope image (×37) using back-scattered electrons, *bce* (**) appeared black-gray and specimen surface in gray-white. (A_1) *m-Ti* specimen; (B_1) *sb-YTZP* specimen; and (C_1) *p-Ti*.

ones,[15] probably due to an increase of the surface area available for adhesion.[15]

The present study clearly demonstrated that implant surface roughness has an important role for early biomaterial integration. The hierarchical structure of the *p-Ti* samples, observed under SEM, resulted in a microporous topography surface able to literally catch the red blood cells. These findings were consistent with a previous report.[21] The present results also suggested that the type of material was able to influence the activation of the common pathways of blood coagulation and of platelet activation. The changes in blood coagulation in this study could be directly correlated to the changes in the surface chemistry induced by the material type. This was evidenced by the difference in contact angle from 48.70° for *Sb-YTZP* down to 38.00° for *p-Ti*.

The statistically significant higher amount of fibrin clot on the *p-Ti* surface than on the *sb-YTZP* or

TABLE 3 Blood Clot Extension on Sample Surfaces

Groups	*n*	Means ($\times 10^7$ µm^2)	Standard Deviations ($\times 10^6$ µm^2)
m-Ti	5	2.97*†	6.68
p-Ti	5	5.64*	6.83
sb-YTZP	15	3.61*†	7.67

*Statistically significant.
†Not statistically significant at $\alpha < 0.05$ and $1 - \beta = 1.00$.
Normality test: passed ($p = .489$); equal variance test: passed ($p = .988$).
One-way ANOVA and Holm-Sidak methods.
ANOVA = analysis of variance; m-Ti = titanium specimens with machined surface; p-Ti = titanium specimens with plus surface; sb-YTZP = yttria tetragonal zirconia polycrystal specimens with sand-blasted surface.

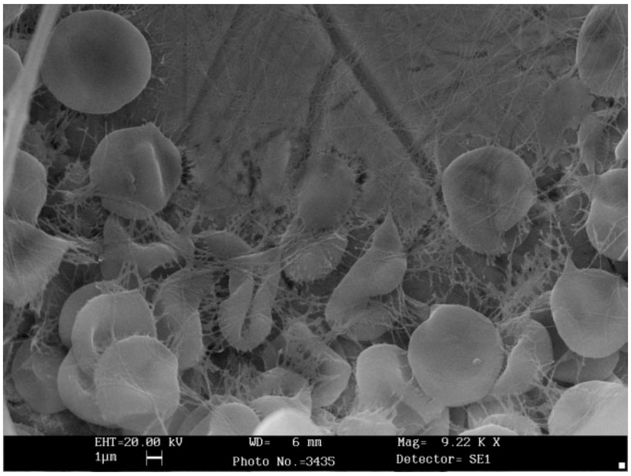

Figure 7 Scanning electron microscope image (×9.220) of machined titanium surface (*m-Ti*) with blood clot. Fibrin filaments are thin and not very extensive; some red blood cells are also visible.

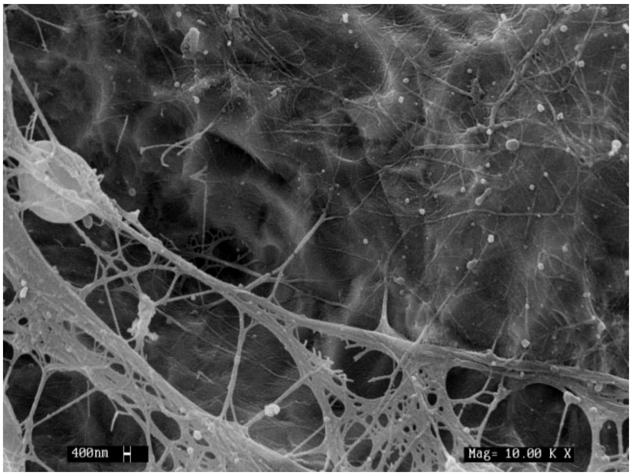

Figure 8 Scanning electron microscope image (×10.000) of sandblasted zirconia surface (*sb-YTZP*) with blood clot. The fibrin scaffold looks like a three-dimensional network; the zirconia surface is visible in the background; two red blood cells trapped in the fibrin scaffold are also visible.

m-Ti surfaces appeared to be related to the three-dimensional arrangement of the fibrin clot among the groups. In the *m-Ti* group, the fibrin network had a two-dimensional extension, with large areas of the metal surface visible among the fibrin filaments (Figure 7), while in the *p-Ti* group, the fibrin appeared like a three-dimensional network (Figure 9). The microscopic morphology of the fibrin clot on the *sb-YTZP* samples appeared to be interesting, which showed very few red blood cells retained inside the three-dimensional fibrin scaffold (Figure 8). It was hypothesized that the implant

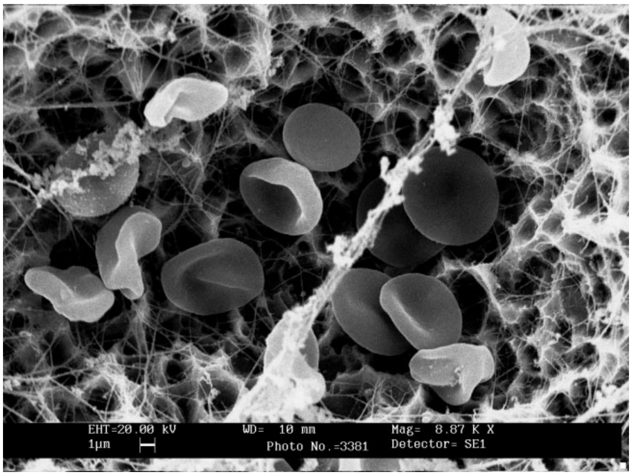

Figure 9 Scanning electron microscope image (×8.870) of plus titanium surface (*p-Ti*) with blood clot. Both fibrin and red blood cells are present. A three-dimensional extensive intricate fibrin network is visible on specimen surface with red blood cells trapped in the fibrin scaffold.

surface microtexture could influence the spatial arrangement of the fibrin while the electronic structure of the material surface was able to influence the chemistry of the coagulation. In fact, the band gap of the zirconia was >5 eV, while the band gap value of titanium was 3.06 ± 0.12 eV, much closer to 1.8 eV of fibrinogen. In some ways, the coagulation process was less effective over the zirconia samples. Comparing the results for *bce* and contact angles (Figure 10), the inverse relation between contact angle and *bce* was evident. *sb-YTZP* showed a higher contact angle and a lower *bce* value. The *bce* value of *sb-YTZP* was slightly more than *m-Ti* and the *Ra* values of the two groups were significantly different. The higher amount of fibrin and the large number of red blood cells should be related to the rate of platelet activation during clot formation, due to a major amount of chemotactic factors released in healing site.[42]

According to Park and Davies,[45] the agglomeration of red cells could be caused by the release of macromolecules by platelets; hence, the presence of red cells could be caused by the activation of platelets. The fibrin three-dimensional structure on the *p-Ti* surface could be related both to the three-dimensional microstructure of this surface and to the closer band gap energy with fibrinogen. Further studies are, however, necessary to clarify this point. As described by Davies,[41] bone healing around dental implants could be divided in osteogenic cell migration, de novo bone formation, and bone remodeling. Osteogenic cell migration and de novo bone formation were two phases of the same process named "contact osteogenesis," with formation of bone directly on the implant surface. The first step of contact osteogenesis was the recruitment of osteogenic cells from perivascular connective tissue; these cells could migrate toward the implant surface using the fibrin scaffold. Interactions between membrane proteins and fibrin were crucial in producing the ameboid movements through the fibrin scaffold. These mechanisms stressed the importance of the fibrin scaffold in the early phases of healing of peri-implant bone. The ability of the implant surface to retain the fibrin attachment during the wound contraction seemed to be of relevant importance in maintaining the pathway for the osteogenic cells to reach the implant surface.[41]

The type, quantity, and activity of adsorbed proteins were influenced by the properties of the biomaterial (surface chemistry and hydrophobicity).[16,46] *p-Ti* surface has been shown to be totally wettable after the first

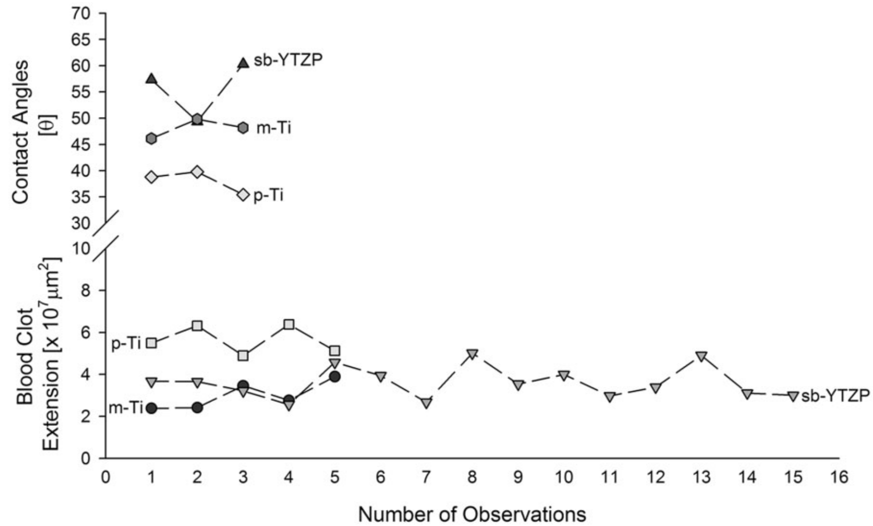

Figure 10 Plot of contact angles *versus* blood clot extension (*bce*). The inverse relation between contact angle and *bce* appear evident. *sb-YTZP* shows both a high-contact angle and a low-*bce* rate. *p-Ti* and vice versa show a low-contact angle and a high-*bce* rate.

emersion cycle.[46] It was hypothesized that there could be a direct correlation of the hierarchical structure of indentations of the *p-Ti* surface and the wetting behavior.[46] Moreover, the presence of the sharp edges observed under SEM on the *p-Ti* surface (Figure 2) could help the adhesion of cells by presenting a differential in the chemistry of the implant surface.[19] The proteins adsorbing to the edge could take up a different shape from those adsorbed to a continuously flat surface.[19]

According to Johnson and colleagues,[44] whole blood instead of anticoagulated blood was used in the present study because anticoagulation substances could modify the blood coagulation cascade.

In conclusion, the results of this in vitro study revealed that the *sb-YTZP* specimens showed, in mean, a significant decrease of *bce* compared with *p-Ti* specimens, while the values of both *Ra* and θ were not statistically different. The increase of the surface microtexture complexity as well as the use of titanium seemed both to determine the formation of a more extensive and three-dimensionally complex fibrin scaffold. Further investigations are necessary to explain the relationships between band gap energy and blood clot formation.

DISCLOSURE

The authors have not received remuneration or other perquisites for personal or professional use from a commercial or industrial agent in direct or indirect relationship to their authorship.

REFERENCES

1. Anderson JM. Biological responses to materials. Annu Rev Mater Res 2001; 31:81–110.
2. Arvidsson S, Askendal A, Tengvall P. Blood plasma contact activation on silicon, titanium and aluminium. Biomaterials 2007; 28:1346–1354.
3. Fiberg B, Grondahl K, Lekholm U, Branemark PI. Long-term follow-up of severely atrophic edentulous mandibles reconstructed with short Brånemark implants. Clin Implant Dent Relat Res 2000; 2:184–189.
4. Vanzillotta PS, Sader MS, Bastos IN, Soares GdeA. Improvement of in vitro titanium bioactivity by three different surface treatments. Dent Mater 2006; 22:275–282.
5. Gorbet MB, Sefton MV. Biomaterial-associated thrombosis: roles of coagulation factors, complement, platelets and leukocytes. Biomaterials 2004; 25:5681–5703.
6. Smith BR, Rinder HM, Rinder CS. Interaction of blood and artificial surfaces. In: Loscalzo JSA, ed. Thrombosis and hemorrhage. Philadelphia: Lippincott, 2003:865–900.
7. Stanford CM. Surface modification of biomedical and dental implants and the processes of inflammation, wound healing and bone formation. Int J Mol Sci 2010; 11:354–369.
8. Hong J, Andersson J, Ekdahl KN, et al. Titanium is a highly thrombogenic biomaterial: possible implications for osteogenesis. Thromb Haemost 1999; 82:58–64.
9. Akagawa Y, Hosokawa R, Sato Y, Kamayama K. Comparison between freestanding and tooth connected partially stabilized zirconia implants after two years' function in monkeys: a clinical and histologic study. J Prosthet Dent 1998; 80: 551–558.
10. Gahlert M, Gudehus T, Eichhorn S, Steinhauser E, Kniha H, Erhardt W. Biomechanical and histomorphometric

comparison between zirconia implants with varying surface textures and a titanium implant in the maxilla of miniature pigs. Clin Oral Implants Res 2007; 18:662–668.

11. Kohal RJ, Weng D, Bächle M, Strub JR. Loaded custom-made zirconia and titanium implants show similar osseointegration: an animal experiment. J Periodontol 2004; 75: 1262–1268.
12. Sennerby L, Dasmah A, Larsson B, Iverhed M. Bone tissue responses to surface-modified zirconia implants: a histomorphometric and removal torque study in the rabbit. Clin Implant Dent Relat Res 2005; 7:13–20.
13. Özkurt Z, Kazazoğlu E. Zirconia dental implants: a literature review. J Oral Implantol 2011; 37:367–376.
14. Oliva J, Oliva X, Oliva JD. Five-year success rate of 831 consecutively placed zirconia dental implants in humans: a comparison of three different rough surfaces. Int J Oral Maxillofac Implants 2010; 25:336–344.
15. Karacs A, Fancsaly JA, Divinyi T, Peto G, Kovach G. Morphological and animal study of titanium dental implant surface induced by blasting and high intensity pulsed Nd-glass laser. Mater Sci Eng C Mater Biol Appl 2003; 23:431–435.
16. Keselowsky BG, Collard DM, Garcia AJ. Surface chemistry modulates focal adhesion composition and signaling through changes in integrin binding. Biomaterials 2004; 25:5947–5954.
17. Lange R, Luthen F, Beck U, Rychly J, Baumann A, Nebe B. Cell-extracellular matrix interactions and physiochemical characteristics of titanium surfaces depend on the roughness of the material. Biomol Eng 2002; 19:255–261.
18. Magnani A, Priamo A, Pasqui D, Barbucci R. Cell behavior on chemically microstructured surfaces. Mater Sci Eng C Mater Biol Appl 2003; 23:315–328.
19. Riehle MO, Dalby MJ, Johnstone H, Macintosh A, Affrossman S. Cell behaviour of rat calvaria bone cells on surfaces with random nanometric features. Mater Sci Eng C Mater Biol Appl 2003; 23:337–340.
20. Kim YH, Koak JY, Chang IT, Wennerberg A, Heo SJ. A histomorphometric analysis of the effects of various surface treatment methods on osseointegration. Int J Oral Maxillofac Implants 2003; 18:349–356.
21. Di Iorio D, Traini T, Degidi M, Caputi S, Neugebauer J, Piattelli A. Quantitative evaluation of the fibrin clot extension on different implant surfaces: an in vitro study. J Biomed Mater Res B Appl Biomater 2005; 74B:636–642.
22. Sul YT, Johansson CB, Roser K, Albrektsson T. Qualitative and quantitative observations of bone tissue reactions to anodised implants. Biomaterials 2002; 23:1809–1817.
23. Buser D, Schenk RK, Steinemann S, Fiorellini JP, Fox CH, Stich H. Influence of surface characteristics on bone integration of titanium implants. A histomorphometric study in miniature pigs. J Biomed Mater Res B Appl Biomater 1991; 25:889–902.
24. Larsson C, Thomsen P, Aronsson BO, et al. Bone response to surface-modified titanium implants: studies on the early tissue response to machined and electropolished implants with different oxide thicknesses. Biomaterials 1996; 17:605–616.
25. Nygren H, Tengvall P, Lundstrom I. The initial reactions of TiO2 with blood. J Biomed Mater Res 1997; 34:487–492.
26. Horbett TA. Principles underlying the role of adsorbed plasma proteins in blood interaction with foreign materials. Cardiovasc Pathol 1993; 2:137–148.
27. Vroman L. Problems in the development of materials that are compatible with blood. Biomater Med Devices Artif Organs 1984; 12:307–323.
28. Sevastianov VI. Role of protein adsorption in blood compatibility of polymers. Crit Rev Biocompat 1988; 4:109–154.
29. Tang L, Eaton JW. Fibrinogen mediates acute inflammatory responses to biomaterials. J Exp Med 1993; 178:2147–2156.
30. Bangham AD. A correlation between surface charge and coagulant action of phospholipids. Nature 1962; 192:1197–1198.
31. Drummond RK, Peppas NA. Fibrinolytic behaviour of streptokinase-immobilized poly(methacrylic acid-g-ethylene) oxide. Biomaterials 1991; 12:356–360.
32. Jackson CM, Nemerson Y. Blood coagulation. Ann Rev Biochem 1980; 49:765–811.
33. Johnson RJ. Complement activation during extracorporeal therapy: biochemistry, cell biology and clinical relevance. Nephtol Dial Transplant 1994; 9:36–45.
34. Siemssen PA, Garred P, Olsen J, Aasen AO, Mollnes TE. Activation of complement, fibrinolysis and coagulation systems by urinary catheters. Effect of time and temperature in biocompatibility studies. Br J Urol 1991; 67:83–87.
35. Mosesson MW. Fibrinogen functions and fibrin assembly. Fibrinolysis Proteol 2000; 14:182–186.
36. Kawase T, Okuda K, Wolff LF, Yoshie H. Platelet-rich plasma-derived fibrin clot formation stimulates collagen synthesis in periodontal ligament and osteoblastic cells in vitro. J Periodontol 2003; 74:858–864.
37. Chen JY, Leng. Y, Tian XB, et al. Antithrombogenic investigation of surface energy and optical bandgap and hemocompatibility mechanism of Ti(Ta(+5))O2 thin films. Biomaterials 2002; 23:2545–2552.
38. Chen X, Mao. S Titanium dioxide nanomaterials: synthesis, properties, modifications, and applications. Chem Rev 2007; 107:2891–2959.
39. Schmoekel H, Schense JC, Weber FE, et al. Bone healing in the rat and dog with nonglycosylated BMP-2 demonstrating low solubility in fibrin matrices. J Orthop Res 2004; 22:376–381.
40. Yucel EA, Oral O, Olgac V, Oral CK. Effects of fibrin glue on wound healing in oral cavity. J Dent 2003; 31:569–575.
41. Davies JE. Mechanisms of endosseous integration. Int J Prosthodont 1998; 11:391–401.

42. Park JY, Gemmel CH, Davies JE. Platelet interactions with titanium: modulation of platelet activity by surface topography. Biomaterials 2001; 22:2671–2682.
43. Nygren H, Stenberg M. Molecular and supramolecular structure of adsorbed fibrinogen and adsorption isotherms of fibrinogen at quartz surfaces. J Biomed Mater Res 1988; 22:1–11.
44. Johnson K, Aaden LA, Choy Y, De Groot E, Greasey A. The proinflammatory cytokine response to coagulation and endotoxin in whole blood. Blood 1996; 87:5051–5060.
45. Park JY, Davies JE. Red blood cell and platelet interactions with titanium implant surfaces. Clin Oral Implants Res 2000; 11:530–539.
46. Rupp F, Scheideler L, Rehbein D, Axmann D, Geis-Gerstorfer J. Roughness induced dynamic changes of wettability of acid etched titanium implant modification. Biomaterials 2004; 25:1429–1438.